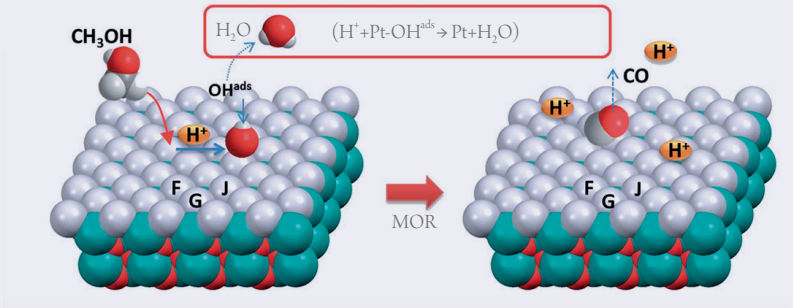

Fig. 4: Bimetallic models of Pt_S/Ru_C NC: Pt on RuO_2 (001) "4×4 RuO_2+ 32 Pt". [Reproduced from Ref. 4]

Figure 4 shows the configuration of Pt_S/Ru_C NC to illustrate the effect of the geometric confinement on the local restructuring in the surface of the core-shell NC during MOR. Chemisorption of CH_3OH on top of the Pt atoms (Pt–CH_3O-H_{ads}) and subsequent decomposition of H^+ from Pt–CH_3OH_{ads} in the core-shell structure proceeds with a small activation energy. The residual CO molecule adhered at both the bridge of the Pt_F–Pt_G sites and the hollow sites after decomposition of H^+ from Pt–CH_3OH_{ads} in the core-shell that elongates the bond between the CO molecule and the sorption sites. This bond weakening leads to substantial dissolution followed by a regrowth of hydrophilic components under mild redox conditions. This geometrical confinement can serve as a highly ordered Pt capsule to protect the core from the redox environment, thus improving the enduring stability of the NC.

These two works not only renew our knowledge about the structural effects of nanocatalysts, apart from the well investigated phenomena of reactivity and durability, but also indicate a new direction to control metallic structure or the core-shell heterostructure, which is the key to achieve a great DMFC fuel cell. (Reported by Yao-Jane Hsu)

This report features the works of Meng-Fan Luo and his co-workers published in ACS Catalysis ***5****, 4726 (2015) and of Tsan-Yao Chen and his co-workers published in J. Mater. Chem. A* ***3****, 1518 (2015).*

References

1. M.-F. Luo, H.-W. Shiu, M.-H. Tien, S. D. Sartale, C. I. Chiang, Y. C. Lin, and Y. J. Hsu, Surf. Sci. **602**, 241 (2008).
2. J. Zhou and D. R. Mullins, J. Phys. Chem. B **110**, 15994 (2006).
3. T.-C. Hung, T.-W. Liao, Z.-H. Liao, P.-W. Hsu, P.-Y. Cai, H. Lee, Y.-L. Lai, Y.-J. Hsu, H.-Y. Chen, J.-H. Wang, and M.-F. Luo, ACS Catal. **5**, 4276 (2015).
4. J.-J. Wang, Y.-T. Liu, I.-L. Chen, Y.-W. Yang, T.-K. Yeh, C.-H. Lee, C.-C. Hu, T.-C. Wen, T.-Y. Chen, and T.-L. Lin, J. Phys. Chem. C **118**, 2253 (2014).
5. T.-Y. Chen, G.-W. Lee, Y.-T. Liu, Y.-F. Liao, C.-C. Huang, D.-S. Lin, and T.-L. Lin, J. Mater. Chem. A **3**, 1518 (2015).

Magnetic Mesocrystals of New Types

Mesocrystals, materials in a new class with nanocrystal superstructures exhibiting directional or translational symmetry, have captured significant attention in the past decade due to their potential for applications of catalytic, electronic, optical, drug-delivery and reaction-precursor applications. Because of their structural nature, the mesocrystals can possess unique properties and functionalities that are distinct from bulk or nano functional materials. Considerable efforts have been made to develop mechanisms of synthesis and to acquire new members of the mesocrystal family, such as oxide, metal and organics, as well as to tailor their various functionalities. In 2015, a research team of Ying-Hao Chu (National Chiao Tung University) demonstrated magnetic mesocrystals of several new types consisting of self-assembled core-shell nanocrystals or nanocrystals embedded in a matrix material via epitaxial growth. The epitaxy enables the alignment of orientations among nanocrystals, forming building blocks of a mesocrystal to enlarge the playground of mesocrystals. According to their recent reports, this team demonstrated a growth method to synthesize self-organized two-dimensional mesocrystals composed of highly oriented magnetic nanocrystals with assistance of shell materials or various matrices. The properties of the mesocrystals were modulated on either varying the core-shell structure or altering the surrounding matrix. To uncover the intriguing functionalities of these mesocrystals, X-ray absorption spectroscopy (XAS) and X-ray magnetic circular dichroism (XMCD) at **BL11A1** were employed to understand the coupling mechanisms between core and shell materials or nanocrystal and matrix, which provide critical insight to tailor the physical properties of mesocrystals.

Considerable efforts have been made to develop mechanisms of synthesis and to acquire new members of the mesocrystal family as well as to tailor their tantalizing functionalities. The challenge to grow core-shell oxide nanocrystals as building blocks for mesocrystals remains in the formation of discrete nanocrystals epitaxially on substrates. In Ref. 1, they employed cobalt oxide (CoO)-cobalt ferrite ($Co_xFe_{3-x}O_4$, CFO) as a model system of self-assembled core-shell building blocks for mesocrystals. CoO is an antiferromagnetic (AFM) material; it can modify the magnetic anisotropy of ferrimagnetic CFO via interfacial exchange coupling. They used $BiCoO_3$/$BiFeO_3$ targets to generate CoO/Fe_3O_4 and Bi_2O_3 species with pulsed-laser deposition (PLD). Fe_3O_4 would notably react further with CoO to form the CFO during the deposition. The greater interfacial energy of Fe_3O_4-STO interfaces plays an essential role to drive Fe_3O_4 to diffuse toward CoO cores with the aid of melted Bi_2O_3. After the deposition, the growth chamber was again evacuated to remove Bi_2O_3, and core-shell mesocrystals were formed. The orientation control of core-shell building blocks can be achieved also with varied morphology and properties of mesocrystals. The magnetic anisotropy strongly reflects the advantages of the orientation control in mesocrystal systems. In addition, the interface of the core-shell mesocrystal can be designed on varying the ratio of core to shell because the exchange coupling at the CFO-CoO interface can modify the magnetic anisotropy of the building blocks and thus the entire mesocrystal. Furthermore, the sequence of core-shell is another parameter to be controlled to tailor the properties of core-shell mesocrystals; CFO(core)-CoO(shell) *inverse* mesocrystals can be fabricated simply on exchanging the deposition sequence of $BiCoO_3$ and $BiFeO_3$.

In this work, as the crystal structures of CoO and CFO are similar, inter-diffusion is expected, which hinders the basic understanding of the mesocrystal system. To provide further information, XAS-XMCD was employed. To determine the value of x in $Co_xFe_{3-x}O_4$ phases, XMCD was applied to determine the valence and magnetic moment of Fe and Co. A magnetic field ± 1 T was applied along the out-of-plane direction of samples and the Poynting vector of X-rays was 30° off the out-of-plane axis. Figures 1(a) and 1(b) show the XMCD results of the CoO and Fe_3O_4 core-

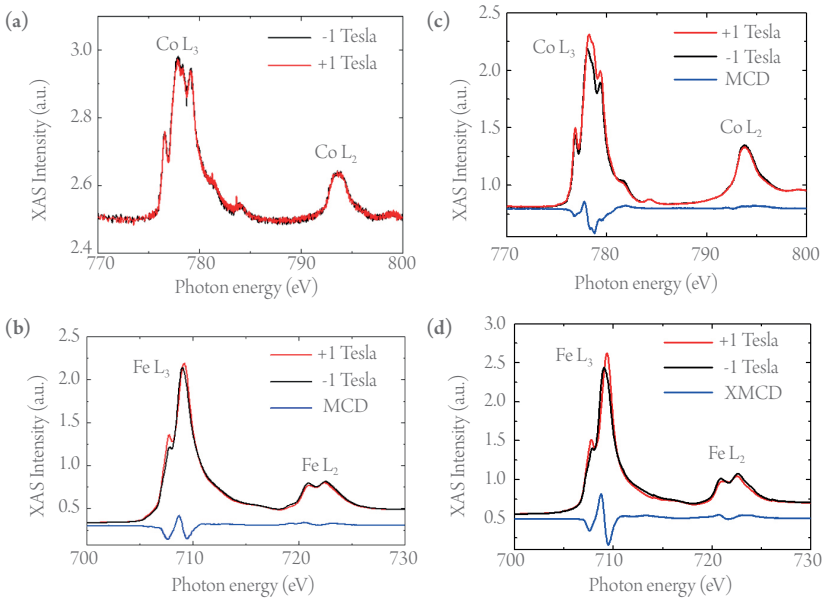

Fig. 1: XMCD of (001)-oriented mesocrystal. (a) Co $L_{2,3}$ edge of CoO core-only mesocrystal. (b) Fe $L_{2,3}$ edge of Fe_3O_4 core-only mesocrystal. (c) Co $L_{2,3}$ edge and (d) Fe $L_{2,3}$ edge of CoO(core)-CFO(shell) core-shell mesocrystal.

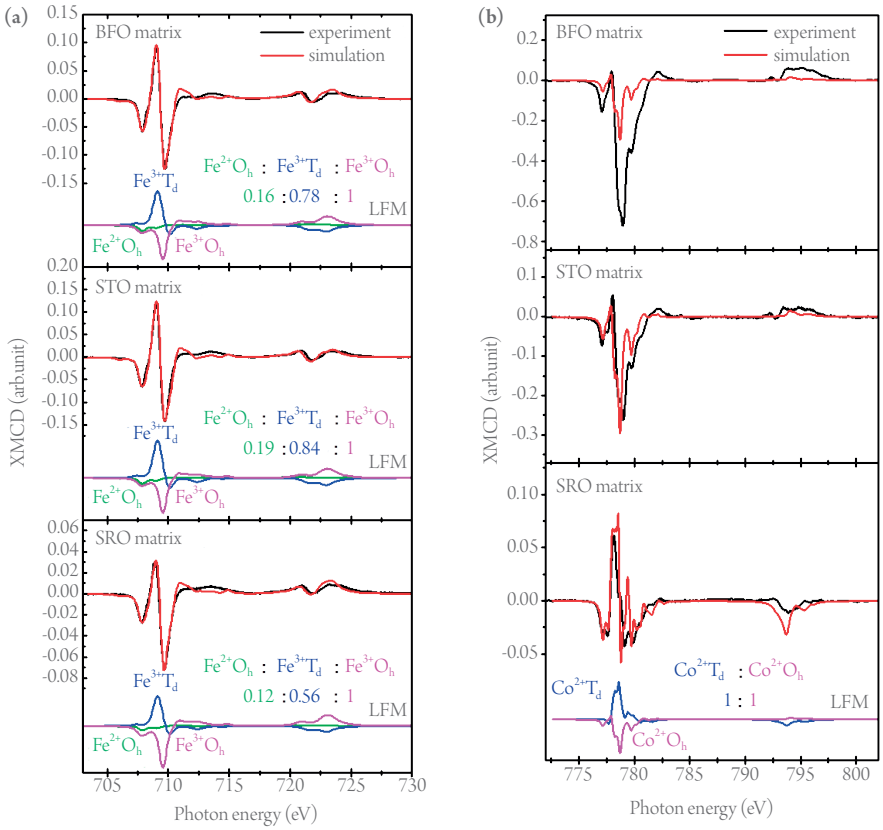

Fig. 2: (a) Co and (b) Fe $L_{3,2}$-edge XMCD spectra extracted from photo-helicity of incident X-rays parallel (μ+) and anti-parallel (μ–) to the direction of magnetization for the CFO mesocrystal in BFO, STO and SRO matrices. By simulating the experimental curves using a LFM model, the ratio of tetrahedral and octahedral sites for Co and Fe cations can be obtained, which shows an obvious redistribution between each cation and a site that is highly correlated to the stress-mediated structural coupling. [Reproduced from Ref. 2.]

only mesocrystals, respectively. The result for the CoO core-only mesocrystal shows typical CoO without net magnetic moment. The result for the Fe_3O_4 core-only mesocrystal shows typical Fe_3O_4 with Fe^{2+} in octahedral and Fe^{3+} in octahedral and tetrahedral sites. Figures 1(c) and 1(d) show the results for a CoO (core)-CFO (shell) mesocrystal. A large magnetic moment of $Co2^{+}$ was found, which is coupled ferromagnetically to Fe^{3+} in octahedral sites and antiferromagnetically to Fe^{3+} in a tetrahedral site. Fe^{2+} nearly disappeared. This fact reveals the formation of CFO with x near one. This result provides crucial information for further building a physical model to explain the tunable properties of the core-shell mesocrystals.

Furthermore, the functionalities of mesocrystals are the collective behaviors of the composed nanocrystals. Tuning the intrinsic properties of the constituent nanocrystals is thus one essential factor to determine the properties of mesocrystals, but the matrix, the other important part of the composite system, has been treated only to assemble nanocrystals into an array with a specific crystallographic orientation. Little attention has been paid to understand the influence of the matrix on the properties of these nanocrystals. To unveil this relation between the matrix and the nanocrystals, self-assembled epitaxial nanocomposites synthesized with PLD served as an example. In these systems, two oxide materials, spinels and perovskites, served as nanopillars and matrix, respectively. The spontaneously assembled nanopillars also possessed a perfectly ordered crystal orientation, which can be viewed as a two-dimensional mesocrystal system. The perovskite matrix can establish a compact connection with the spinel mesocrystal through the bridging of octahedral sites, which strongly affects the structural and physical properties of the mesocrystals. The matrix materials thus become important as they provide additional degrees of freedom to tailor the crystal orientations and physical properties of the mesocrystal, which cannot be observed in those mesocrystals within the organic or polymer matrices. In Ref. 2, spinel CFO and several perovskties ($BiFeO_3$ (BFO), $PbTiO_3$ (PTO), $SrTiO_3$ (STO), and $SrRuO_3$ (SRO)) were chosen. When CFO and perovskite materials were codeposited on perovskite substrates, CFO naturally formed mesocrystals because of the large surface energy at the interface of spinel and perovskite. The CFO mesocrystal was found to undergo varied out-of-plane compressive strain states when embedded in several commonly adopted perovskite matrices. The variation of the strain state in the CFO mesocrystal also alters its magnetic properties such as magnetic anisotropy or the origin of the magnetic moment on an atomic scale. These results indicate that a state of increased strain of the CFO mesocrystal drives the variation of k_{12}, which has been observed in those cases of off-stoichiometric CFO through the cation site-exchange of Co and Fe ions. There is hence expected to be a strong correlation between strain state and cation redistribution in a CFO mesocrystal. This speculation was verified on performing XMCD measurements; this technique is useful to understand the charge, site symmetry and origin of magnetic moments on an atomic scale. Three samples selected for XMCD measurement were the CFO mesocrystals with BFO, STO and SRO matrices, which represent the strain-free, medium strain,

and highly strained states, respectively. By applying a site simulation based on a ligand-field model, XMCD spectra at Fe $L_{2,3}$ edges for these three samples (Fig. 2(a)) exhibit two negative signals and one positive signal, which correspond to Fe^{2+} and Fe^{3+} cations at octahedral (O_h) sites, and Fe^{3+} cations at tetrahedral (T_d) sites, respectively. In addition, the sample with a SRO matrix exhibits a decreased intensity of signal in Fe^{3+} T_d sites and an increased intensity in Fe^{3+} O_h sites relative to the other two samples, revealing that more Fe^{3+} cations prefer to occupy the O_h sites in this case. In contrast, XMCD spectra measured at Co $L_{2,3}$ edges (Fig. 2(b)) show a significant discrepancy among these three samples. Although Co XMCD measured from the samples with BFO and STO matrices showed the same line shape and were consistent with the reference XMCD of Co^{2+} at O_h sites, the BFO matrix possessed a much larger XMCD signal than the other two. The simulation of the XMCD spectrum measured from the sample with a SRO matrix reveals a mixture of Co^{2+} cations at T_d and O_h sites. The existence of Fe^{2+} O_h sites and Co^{2+} T_d sites indicates that site exchange occurs in these systems because a strain effect or oxygen vacancies can readily break the symmetry and redistribute cations and charges. Based on the results of site simulation, the ratio of Fe^{3+} T_d sites and O_h sites was obtained as ~ 0.78 for nearly strain-free CFO, ~ 0.84 for moderately strained CFO and ~ 0.56 for highly strained CFO. The Co^{2+} cations occupy solely the O_h sites for nearly strain-free and moderately strained cases, which retain similar electronic structures near those of the CFO references. The highly strained CFO has a ratio of Co^{2+} T_d sites and O_h site near one.

The work of this team delivers new concepts to design functional core-shell mesocrystals and stress-mediated functionalities of mesocrystals. The results from XAS-XMCD were a key to reveal the insight of these studies. (Reported by Ying-Hao Chu)

This report features the work of Ying-Hao Chu and his co-workers published in Small ***33,*** *4117 (2015) and Sci. Rep.* ***5,*** *12073 (2015).*

References

1. S. C. Liao, Y. L. Chen, W. C. Kuo, J. Cheung, W. C. Wang, X. Cheng, Y. Y. Chin, Y. Z. Chen, H. J. Liu, H. J. Lin, C. T. Chen, J. Y. Juang, Y. L. Chueh, N. Valanoor, Y. H. Chu, and C. H. Lai, Small **11**, 4117 (2015).
2. H. J. Liu, Y. Y. Liu, C. Y. Tsai, S. C. Liao, Y. J. Chen, H. J. Lin, W. F. Hsieh, C. H. Lai, J. Y. Li, C. T. Chen, Q. He, and Y. H. Chu, Sci. Rep. **5**, 12073 (2015).

Itinerant Hole Carriers Mediate Local Magnetic Moments

Diluted magnetic semiconductors (DMS) have received much attention due to the possibility of utilizing both charge and spin degrees of freedom in electronic devices.[1,2] To realize functional spintronic devices, it is important to have full control of the carrier density and ferromagnetic Curie temperature (T_C). A newly found DMS, $Ba_{1-x}K_x(Zn_{1-y}Mn_y)_2As_2$ (Mn-$BaZn_2As_2$),[3] is isostructural with iron-based superconductors[4] of type "122" and has a T_C up to 230 K.[5] This material has an advantage that the charge-reservoir Ba layer and the ferromagnetic ZnAs layer are spatially separated, as shown in Fig. 1, which independently allows control of the amount of hole carriers by K substitution into the Ba layer and that of magnetic elements on substituting Mn into the ZnAs layer. As DMS in this series show great possibilities for next-generation spintronic devices, Suzuki *et al.*[6] investigated the electronic and magnetic structures of Mn-$BaZn_2As_2$ and compared them with archetypal Mn-doped DMS materials such as $Ga_{1-x}Mn_xAs$.

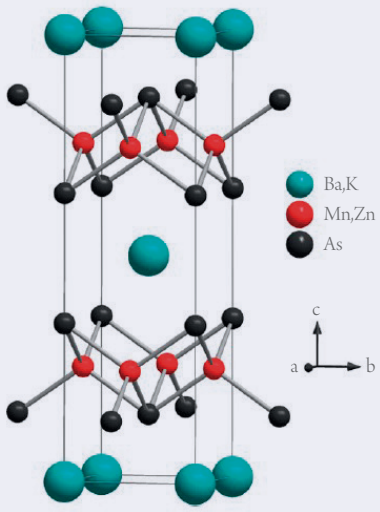

Fig. 1: Crystal structure of Mn-$BaZn_2As_2$ (structure of type $ThCr_2Si_2$, space group *I4/mmm*). [Reproduced from Ref. 4]

They recorded X-ray absorption spectroscopy (XAS) and resonant photoemission spectroscopy (RPES) of $Ba_{0.7}K_{0.3}(Zn_{0.85}Mn_{0.15})_2As_2$ (Mn-$BaZn_2As_2$) polycrystalline samples at **BL11A1** of the TLS and at BL-2C of Photon Factory, respectively. The samples were filed *in situ* before the measurements to ensure fresh surfaces.

Figure 2 shows the Mn $L_{2,3}$-edge XAS of Mn-$BaZn_2As_2$ compared with those of reference Mn materials. The energy of the main Mn L_3-edge XAS signal shows the valence of the Mn atom. The main Mn L_3-edge XAS signal of Mn-$BaZn_2As_2$ is located above that of Mn metal, below that of $LaMnO_3$ (Mn^{3+}), and the same as of Mn^{2+} compounds; this result shows the Mn atom in Mn-$BaZn_2As_2$ to take valence 2+. The Mn line shape of the $L_{2,3}$-edge XAS reflects the localized nature of Mn *3d* states; as the multiplet structures become clearer, the Mn *3d* electronic structures become more localized. The XAS line shape of Mn-$BaZn_2As_2$ is intermediate between those of two DMS systems, $Ga_{0.922}Mn_{0.078}As$ (GaMnAs) and $Ga_{0.958}Mn_{0.042}N$ (GaMnN). The shoulder structures at 640 and 643 eV are more pronounced than in GaMnAs and weaker than in GaMnN. This effect indicates that Mn *3d* orbitals strongly hybridize with the surrounding As *4p* orbitals as in GaMnAs and GaMnN; the strength of hybridization is greater than in GaMnAs but weaker than in GaMnN.

To extract the local electronic structures of the doped Mn, they performed RPES experiments using photon energies at the Mn L_3-edge. The *3d* partial density of states (PDOS) of a transition metal in solids was deduced on taking the difference of valence-band photoemission spectra between on-resonant and off-resonant photon energies. For Mn-$BaZn_2As_2$, on-resonant and off-resonant photon energies at Mn L_3-edge are estimated to be 635 and 638.5 eV from Mn L_3-edge XAS, shown in Fig. 3(a). By subtracting the off-resonant spectra from the on-resonant spectra, they deduced the PDOS of Mn *3d* orbitals as shown in Fig. 3(b). The DOS is small at E_F, finite between -2 eV and E_F, and has a maximum at -4 eV. The deduced Mn *3d* PDOS is compared with that of $Ga_{0.957}Mn_{0.043}As$[7] in Fig. 3(c); the overall spectral shapes are similar. This result indicates that the electronic states of doped Mn are alike in these two DMS systems; the similarity originates from the same chemical valence 2+ of the Mn atoms and the tetrahedral coordination with the As *4p* orbitals. Holes are thus predominantly introduced into the valence band composed mainly of As *4p* states; the local magnetic moments with $S = 5/2$ are formed there in the presence of Hund's coupling between electrons of the d^5 configuration.